International Journal of Solids and Structures 51 (2014) 2491–2503

Contents lists available at ScienceDirect

International Journal of Solids and Structures

journal homepage: www.elsevier.com/locate/ijsolstr

In-plane elastic wave propagation and band-gaps in layered functionally graded phononic crystals

S.I. Fomenko [a], M.V. Golub [a,*], Ch. Zhang [b], T.Q. Bui [b], Y.-S. Wang [c]

[a] Institute for Mathematics, Mechanics and Informatics, Kuban State University, Krasnodar 350040, Russia
[b] Chair of Structural Mechanics, Department of Civil Engineering, University of Siegen, Paul-Bonatz Strasse 9-11, D-57076 Siegen, Germany
[c] Institute of Engineering Mechanics, Beijing Jiaotong University, Beijing 100044, PR China

ARTICLE INFO

Article history:
Received 10 November 2013
Received in revised form 15 March 2014
Available online 27 March 2014

Keywords:
Functionally graded materials
Phononic crystals
Laminates
Elastic waves
Wave transmission
Band-gaps
Transfer matrix method

ABSTRACT

In-plane wave propagation in layered phononic crystals composed of functionally graded interlayers arisen from the solid diffusion of homogeneous isotropic materials of the crystal is considered. Wave transmission and band-gaps due to the material gradation and incident wave-field are investigated. A classification of band-gaps in layered phononic crystals is proposed. The classification relies on the analysis of the eigenvalues of the transfer matrix for a unit-cell and the asymptotics derived for the transmission coefficient. Two kinds of band-gaps, where the transmission coefficient decays exponentially with the number of unit-cells are specified. The so-called low transmission pass-bands are introduced in order to identify frequency ranges, in which the transmission is sufficiently low for engineering applications, but it does not tend to zero exponentially as the number of unit-cells tends to infinity. A polyvalent analysis of the geometrical and physical parameters on band-gaps is presented.

1. Introduction

Functionally graded materials (FGMs) are advanced composites consisting of two or more material phases, characterized by a gradual variation in composition and structure in some spatial directions. The concept of FGMs was introduced in 1984 by a group of material scientists in Japan (Woo and Meguid, 2001; Shen, 2009). One of the superior properties of the FGMs compared to the classical composites is that the continuous gradation in material properties can overcome the interfacial problems typical for most layered composite structures. Owing to their great advantages in a variety of engineering applications, FGMs are essentially designed to take advantages of desirable characteristics of each of the constituent phases.

In recent years, there has been a great deal of works on the analysis of propagation of elastic waves in periodic composite structures or phononic crystals. Phononic crystals are functional composite materials composed of periodic arrays of two or more materials with different material properties and mass densities. In general, the periodicity of phononic crystals may be in one-, two-, or three dimensions with different scatterers, respectively. By owning to the great advantages in a broad range of engineering applications, the wave propagation phenomena in composite materials and structures particularly play an important role in design of new devices in such engineering applications. Basically, the most important properties of phononic crystals lie in the mechanical or acoustical waves, which have specific frequency ranges in which they cannot propagate within the periodic structures. Thus, the frequency ranges that are forbidden for wave propagation are usually called phononic band-gaps or stop-bands, and the occurrence of such band-gaps in periodic elastic structures is caused by the multiple wave scattering at the interfaces between different materials (Brillouin, 1946; Maldovan and Thomas, 2009).

The potential of the methods based on elastic waves for damage detection was demonstrated last century (Viktorov, 1967; Achenbach, 1973; Alleyne and Cawley, 1992). Ultrasonic non-destructive methods require precise and accurate wave excitation and signal reception techniques, which can be realized in particular by the introduction of special elements like phononic crystals with good filtering properties into the actuators and sensors. An example is the acoustic sensor system using resonances of two-dimensional (2D) phononic crystals made up of a steel plate having two regular arrays of holes and a cavity in-between (Zubtsov et al., 2012). Since one-dimensional (1D) phononic crystals or multilayered periodic laminates can be fabricated more easier than two-dimensional (2D) and three-dimensional (3D) phononic crystals, they should be

* Corresponding author. Tel.: +7 9628654432.
E-mail addresses: sfom@yandex.ru (S.I. Fomenko), m_golub@inbox.ru (M.V. Golub), c.zhang@uni-siegen.de (Ch. Zhang), bui-quoc@bauwesen.uni-siegen.de (T.Q. Bui), yswang@bjtu.edu.cn (Y.-S. Wang).

http://dx.doi.org/10.1016/j.ijsolstr.2014.03.017
0020-7683/

investigated in details due to their novel acoustic properties, which have potential engineering applications (Saini et al., 2007). An experimental investigation of phononic band-gaps for a normal wave incidence in a 1D periodic SiO_2/poly (methyl methacrylate) multilayered film at gigahertz frequencies using Brillouin spectroscopy was performed by Gomopoulos et al. (2010). Though many works have been performed on phononic crystals, design of an optimal phononic crystal remains a complex task and elastic wave propagation in 1D phononic crystals is not fully understood yet. The present study aims at developing efficient and accurate methods for fast calculations of band-gaps, which can be applied in the optimization procedure in order to design 1D FGM phononic crystals with demanded properties, and for reliable investigations of the corresponding wave phenomena.

Many previous efforts have particularly been devoted to the simulation and analysis of wave propagation and scattering problems in FG materials and structures (Liu et al., 1991; Sobczak and Drenchev, 2013; Jha et al., 2013). Besides purely numerical methods, including finite difference time domain method (Berezovski et al., 2003; Vollmann et al., 2006), finite element method (Chakraborty and Gopalakrishnan, 2003; Santare et al., 2003) and hybrid numerical methods (Liu et al., 1991; Han et al., 2001) that are more suitable for finite FGM bodies, there are several semi-analytical approaches based on the solution of boundary-value problems in spatial Fourier transform domains (Babeshko et al., 1987; Liu et al., 1999). The semi-analytical approaches can be classified into two groups for convenience. The first group involves explicit mathematical models of FGMs such as the direct integration of differential equations with variable coefficients (Sato, 1959), including modulating function method for Green's matrix (Babeshko et al., 1987) and Peano expansion method for matricants (Shuvalov et al., 2005). The methods from the second group are based on the approximation of an FG layer by a set of sub-layers in which the displacement vectors have explicit expressions. For example, approximations of continuous elastic moduli within the layer by different functions (step-wise, exponential, linear or special power-law) (Liu et al., 1999; Ke and Wang, 2006; Matsuda and Glorieux, 2007; Ting, 2011) and the propagator technique (Gilbert, 1983; Kutsenko et al., 2013) have been used. The simplest layer model (LM) was proposed by using step-wise approximation with homogeneous elastic sub-layers.

Among the most popular methods for layered medium is the transfer matrix method that dates back to the works of Thomson (1950), Petrashen (1952) and Haskell (1953). The LM in conjunction with the T-matrix method seems to be more convenient for numerical calculations of band-gaps in 1D multilayered FG phononic crystals because of fast implementation. However, the equivalence of the LM and the explicit models of the FG layer is not so evident since the explicit models presuppose the first derivatives of the material properties in the governing equations which is excluded in the LM. For example, the replacement of FGMs by a set of homogeneous sub-layers is poor for static problems of indentation (Aizikovich et al., 2011). On the other hand, a comparative analysis of Green's matrixes and surface waves derived by both LM method and the direct integration method with modulating functions have been implemented for in-plane problem in Glushkov et al. (2012). The study has shown that the LM with sufficient number of sub-layers is suitable for the investigation of bulk and surface waves in the layered media. Both of these two approaches have been used also in Golub et al. (2012a), where the efficiency of the LM has been proved in order to analyze SH wave propagation in FG phononic crystals and a brief review on the methods applied to simulate wave motion in layered composites is given. The approaches have been applied to investigate time-harmonic elastic in-plane shear waves propagating in periodically laminated composites with functionally graded interlayers.

Functionally graded (FG) phononic crystals may have elastic properties varying continuously through advanced fabrication technologies such as sputtering, pressing, sintering etc. Besides, a continuous elastic property may appear because of the diffusion processes in the processing of dissimilar layers. Wu et al. (2009) studied the propagation of elastic waves in 1D phononic crystals with FGMs varying with a power-law function. They used the spectral finite element and the transfer matrix methods as main tools to analyze band-gaps and to investigate the effects of various parameters on the wave band-gaps in FG inter-layers structures. Two different power laws were used to describe the property variation of the FG interlayers within the unit-cell, and in conjunction with the transfer matrix method the wave reflection and transmission, band-gaps were investigated. More recently, Su et al. (2012) studied the influences of the material parameters, material composition, and geometrical parameters on the band-gaps of 1D FG phononic crystals by using the plane-wave expansion method. Golub et al. (2013) analyzed the wave propagation in FG treated by recursion relations and effective boundary conditions.

In our previous work (Golub et al., 2012a), SH wave propagation in layered FG elastic phononic crystals has been investigated. In this paper we extend and further develop our methods for efficient and accurate modeling of in-plane P- and SV-wave propagation in FG periodic laminates by using the explicit FG and the multilayer models. Effects of the geometrical and material parameters of the FG phonic crystals on the wave transmission and band-gaps are analyzed in details. The extension of the transfer matrix method to the considered in-plane wave propagation problem is not straightforward due to the numerically accumulating error arising during matrix multiplications. In order to solve this problem a semi-analytical representation for the transmission coefficient is derived. The analysis of the asymptotics of the semi-analytical representation shows different types of band-gaps and gives a criteria for stop-band calculations using eigenvalues of the transfer matrix for a unit-cell.

2. In-plane wave propagation in a layered periodic structure

2.1. Statement of the problem

The propagation of plane time-harmonic elastic P- and waves in a periodically layered media or phononic crystal (PnCr) composed of N identical elastic unit-cells between two identical elastic half-planes is considered. The Cartesian coordinates (x, z) are introduced in such a way that the x-axis is parallel to the interfaces of the phononic crystal and the origin of the coordinate system is on the lower boundary of the structure (Fig. 1). Each of the N unit-cells is composed of two isotropic elastic layers (A and B) and two functionally graded (FG) interlayers between them so that the elastic properties of the whole unit-cell are continuous (Fig. 2(a)). The property variation in the local Cartesian coordinate system of the kth unit-cell of thickness H parallel to the x-axis is described by the following functions as shown in Fig. 2(c)

$$P(z)=\begin{cases} P_A, & z\in[0,h_A],\\ (P_B-P_A)\left(\frac{z-h_A}{h_F}\right)^n+P_A, & z\in[h_A,h_A+h_F],\\ P_B, & z\in[h_A+h_F,h_A+h_F+h_B],\\ (P_B-P_A)\left(\frac{H-z}{h_F}\right)^n+P_A, & z\in[h_A+h_F+h_B,H]. \end{cases} \tag{1}$$

Here the function $P(z)$ denotes an appropriate material property with P_A and P_B being the boundary values corresponding to the mass density or the Lamé constants of the materials A and B (density ρ_A, ρ_B or Lamé constants λ_A, λ_B and μ_A, μ_B), h_A and h_B are the thicknesses of the homogenous layers, h_F is the thickness of the

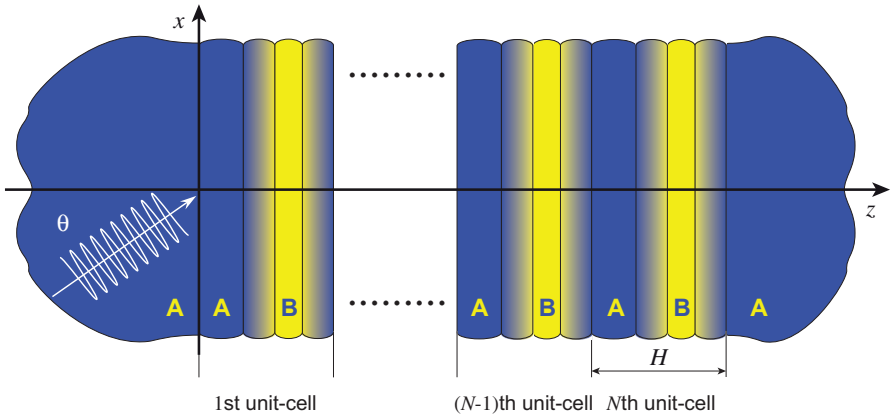

Fig. 1. The geometry of the problem.

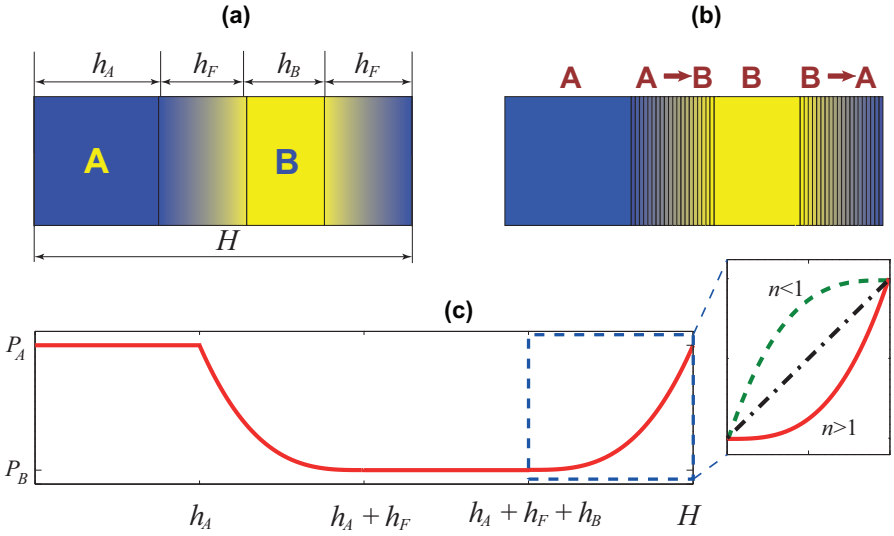

Fig. 2. The unit-cell of the FG phononic crystal (a), its approximation as a multi-layered medium (b), and power law of the material property variation (c).

FG interlayers, and $H = h_A + h_B + 2h_F$ is the thickness of the unit-cell. In this investigation, the exponent of the power law $n = 3$ in Eq. (1) is used. The PnCr is composed of N unit-cells which take the regions $a_{k-1} \leqslant z \leqslant a_k$ $(k = 1, 2, \ldots, N)$ sequentially while the PnCr occupies the total thickness $0 \leqslant z \leqslant N \cdot H$. The used material constants are given in Table 1 (Wu et al., 2009).

2.2. Governing equations and mathematical model

The governing time-harmonic elastodynamic equations with respect to the displacement vector $\mathbf{u} = \{u_x, u_z\} = \{u_1, u_2\}$ in an elastic media with the mass density ρ are the following partial differential equations

$$\sigma_{ij,j} + \rho\omega^2 u_i = 0, \quad i,j = 1,2, \tag{2}$$

where the stress tensor σ_{ij} is expressed in terms of the displacements u_i and Lamé elastic constants λ and μ, which are functions of z

$$\sigma_{ij} = \lambda u_{k,k}\delta_{ij} + \mu(u_{i,j} + u_{j,i}).$$

Here the tensorial index notations are used for the summation and derivative operators and δ_{ij} is the Kronecker delta.The displacements u_i and the stresses σ_{ij} are continuous on all the interfaces of the layered structure, i.e.,

$$\begin{aligned} &\Delta u_1|_{z=z_n} = 0, \quad \Delta u_2|_{z=z_n} = 0, \\ &\Delta\sigma_{12}|_{z=z_n} = 0, \quad \Delta\sigma_{22}|_{z=z_n} = 0, \end{aligned} \tag{3}$$

where $\Delta f(z)|_{z=a} = \lim_{h\to 0}[f(a+h) - f(a-h)]$ denotes the jump of the function $f(z)$ at the interface $z = a$.

The displacements can be expressed in terms of the longitudinal wave and the transverse wave potentials φ and ψ as

$$u_1 = \partial\varphi/\partial z + \partial\psi/\partial x, \quad u_2 = \partial\varphi/\partial x - \partial\psi/\partial z.$$

The wave potentials in a homogeneous elastic medium satisfy the following wave equations

$$\Delta\varphi + \varkappa_P^2\varphi = 0, \quad \Delta\psi + \varkappa_S^2\psi = 0. \tag{4}$$

Table 1
Elastic constants and mass density of the laminated composite.

Notation	Materials	Density (kg/m^3)	Young's modulus (GPa)	Poisson's ratio
A	Alumina	4000	400	0.231
B	Aluminium	2700	70	0.33

Here $\varkappa_P = \omega\sqrt{\rho/(\lambda+2\mu)}$ and $\varkappa_S = \omega\sqrt{\rho/\mu}$ are the wavenumbers of the longitudinal and the transverse waves.

Let us consider the motion of the layered periodic structure excited by time-harmonic plane waves incoming from the plane $z<0$ with the wavenumber α

$$\varphi(x,z,t) = \varphi(z)\exp(\mathrm{i}\alpha x - \mathrm{i}\omega t) \quad \text{and}$$
$$\psi(x,z,t) = \psi(z)\exp(\mathrm{i}\alpha x - \mathrm{i}\omega t),$$

where $\varphi(z)$ and $\psi(z)$ are the complex amplitudes of the wave potentials, and ω is the circular frequency. Since $\varphi(z)$ and $\psi(z)$ satisfy the wave equations (4), the wave potentials can be expressed as

$$\begin{aligned}\varphi(z) &= a_1\exp(\mathrm{i}q_L z) + a_3\exp(-\mathrm{i}q_L z),\\ \psi(z) &= a_2\exp(\mathrm{i}q_T z) + a_4\exp(-\mathrm{i}q_T z),\end{aligned} \tag{5}$$

$$q_L = \sqrt{\varkappa_P^2 - \alpha^2}, \quad q_T = \sqrt{\varkappa_S^2 - \alpha^2}.$$

The coefficients a_i in Eq. (5) depend on the number of the unit-cells and the layer property in such a way to satisfy the continuity conditions (3). On the other hand, the coefficients a_i in (5) for the upper ($z > N\cdot H$) and the lower ($z<0$) half-plane are determined in a different way. In the lower half-plane we assume $a_1 = \delta_L$ and $a_2 = \delta_T$, while a_3 and a_4 are amplitudes of the plane waves reflected by the phononic crystal structure. Correspondingly, in the upper half-space $a_3 = a_4 = 0$ and a_1, a_2 are the wave transmission coefficients.

For pure P- or SV-waves, the corresponding quantities should be chosen as $\delta_L = 1$ and $\delta_T = 0$ or $\delta_L = 0$ and $\delta_T = 1$. For convenience, let us consider a plane time-harmonic elastic wave incident at an angle θ to the z-axis and from $z = -\infty$

$$\mathbf{u}_{inc}(x,z,t) = \mathbf{u}_{inc}(z)\mathrm{e}^{\mathrm{i}\varkappa_0\sin\theta x - \mathrm{i}\omega t}, \quad z\leqslant 0, \tag{6}$$

where $\varkappa_0$ is the wavenumber of the incoming P-wave ($\varkappa_0 = \varkappa_{P,A}$) or SV-wave ($\varkappa_0 = \varkappa_{S,A}$) in the lower half-plane of the material A, $\mathbf{u}_{inc}(z)$ is the complex amplitude of the incident wave that can be expressed in terms of the wave potentials $\varphi_{inc}(z) = \exp(\mathrm{i}\varkappa_{P,A}\cos\theta z)$ or $\psi_{inc}(z) = \exp(\mathrm{i}\varkappa_{S,A}\cos\theta z)$ correspondingly. The time-dependent factors are omitted below and only the complex amplitudes are used for simplicity.

The wave-fields in all homogeneous isotropic sub-layers $z_{k-1} < z < z_k$ are superpositions of plane P- and SV-waves with the wavenumbers $\varkappa_{Lk}$ and $\varkappa_{Tk}$. The angles of the refracted P- and SV-waves θ_{Lk} and θ_{Tk} in the considered sub-layer satisfy the following Snell's law (Grinchenko and Meleshko, 1981; Brekhovskikh and Godin, 1998)

$$\varkappa_{Lk}\sin\theta_{Lk} = \varkappa_{Tk}\sin\theta_{Tk} = \varkappa_0\sin\theta.$$

In general cases, θ_{Lk} and θ_{Tk} are complex-valued and multivalent functions of the incidence angle θ. The correct branches should be chosen by using the principle of bounded energy absorption as

$$\mathrm{Re}[q_{sk}] \geqslant 0, \quad \mathrm{Im}[q_{sk}] \geqslant 0, \quad s = L, T,$$

where $q_{Lk} = \varkappa_{Lk}\cos\theta_{Lk}$ and $q_{Tk} = \varkappa_{Tk}\cos\theta_{Tk}$.

2.3. Transfer matrix of a homogeneous elastic sub-layer

The transfer matrix (T-matrix) method gives a simple expression describing elastic wave motion in a homogeneous elastic sub-layer. The relation between the wave-fields on the two boundaries of the sub-layer can be expressed in terms of the T-matrix and the generalized state vector $\mathbf{v} = \{u_1, u_2, \sigma_{12}, \sigma_{22}\}$. The generalized state vector for the kth sub-layer has matrix representations that can be obtained by substituting Eq. (5) into the expressions for the displacement vector u_i and the stress tensor σ_{ij} in terms of wave potentials as

$$\mathbf{v}(z) = \mathbf{M}_k\mathbf{E}_k(z - z_{k-1})\mathbf{a} = \mathbf{T}(z, z_{k-1})\mathbf{v}(z_{k-1}), \quad z\in[z_{k-1}, z_k]. \tag{7}$$

The representation (7) depends on the generalized vector $\mathbf{a}$ describing the wave-field at the boundary z_{k-1} of the sub-layer. The vector $\mathbf{a} = \{a_1, a_2, a_3, a_4\}$ consists of the wave amplitude coefficients introduced in a way similar to Eq. (5) that can be expressed via $\mathbf{v}(z)$ at any fixed z. By fixing $z = z_{k-1}$ the T-matrix in Eq. (7) has the following form

$$\mathbf{T}(z, z_{k-1}) = \mathbf{M}_k\mathbf{E}_k(z - z_{k-1})\mathbf{M}_k^{-1}. \tag{8}$$

The T-matrix can be expressed explicitly in terms of the coordinate z, the elastic constants, the frequency and the angle θ of an incident wave, see Aki and Richards (2002) and Chen and Wang (2007) for more details.

In Eqs. (7) and (8), the matrix $\mathbf{M}_k$ is composed of four column-vectors

$$\mathbf{M}_k = \left(\mathbf{b}_1^+ \vdots \mathbf{b}_2^+ \vdots \mathbf{b}_1^- \vdots \mathbf{b}_2^-\right), \tag{9}$$

$$\mathbf{b}_1^\pm = \left\{\mathrm{i}\varkappa_{Lk}\sin\theta_{Lk}, \pm\mathrm{i}\varkappa_{Lk}\cos\theta_{Lk}, \mp\mu_k\varkappa_{Lk}^2\sin 2\theta_{Lk}, -\mu_k\varkappa_{Tk}^2\cos 2\theta_{Tk}\right\}^T,$$
$$\mathbf{b}_2^\pm = \left\{\pm\mathrm{i}\varkappa_{Tk}\cos\theta_{Tk}, -\mathrm{i}\varkappa_{Tk}\sin\theta_{Tk}, -\mu_k\varkappa_{Tk}^2\cos 2\theta_{Tk}, \pm\mu_k\varkappa_{Tk}^2\sin 2\theta_{Tk}\right\}^T.$$

The matrix $\mathbf{E}_k(z) = \mathrm{diag}\{\exp[\mathrm{i}q_{Lk}z], \exp[\mathrm{i}q_{Tk}z], \exp[-\mathrm{i}q_{Lk}z], \exp[-\mathrm{i}q_{Tk}z]\}$ in Eqs. (7) and (8) is a diagonal matrix composed of the exponentials.

2.4. Transfer-matrix method for phononic crystals with homogeneous elastic layers and eigenvalues of the T-matrix

The wave transmission and reflection coefficients for a layered phononic crystal structure are determined from the continuity conditions of the stresses and displacements at the interfaces of the sub-layers. The T-matrix method is used for this purpose (Aki and Richards, 2002), where the total T-matrix for the whole layered periodic structure is composed of N T-matrices of the unit-cells, i.e., $\mathbf{T} = \mathbf{T}_c^N$ is a power function of the 4×4 matrix $\mathbf{T}_c$. If the unit-cell consists of L sub-layers then the transfer matrix $\mathbf{T}_c = \mathbf{T}_L\cdot\mathbf{T}_{L-1}\cdot\ldots\cdot\mathbf{T}_2\cdot\mathbf{T}_1$ is a composition of the T-matrices for each sub-layer. Using Jordan basis of the matrix $\mathbf{T}_c$, the total T-matrix of the phononic crystal can be expressed as

$$\mathbf{T} = \mathbf{G}^{-1}\mathbf{\Lambda}^N\mathbf{G},$$

where $\mathbf{G}$ is a change-of-basis matrix to the Jordan normal form $\mathbf{\Lambda} = \mathrm{diag}\{1/\lambda_1, 1/\lambda_2, \lambda_1, \lambda_2\}$ of the matrix $\mathbf{T}_c$.

The amplitude coefficients of the refracted and transmitted P- and SV-waves in the half-planes of the considered layered periodic structure are denoted by (r_L, t_L) and (r_T, t_T) accordingly. The displacement vector in the half-planes

$$\mathbf{u} = \begin{cases}\mathbf{u}_{inc} + r_L\mathbf{u}_{L0}^- + r_T\mathbf{u}_{T0}^-, & z\leqslant 0,\\ t_L\mathbf{u}_{LN}^+ + t_T\mathbf{u}_{TN}^+, & z\geqslant NH\end{cases}$$

is expressed by the displacement vectors $\mathbf{u}_L^\pm$ and $\mathbf{u}_T^\pm$ of plane P- and SV-waves in the lower ($-$) and upper ($+$) half-planes. The continuity conditions at the interfaces between the half-planes and the phononic crystal structure lead to the equation

$$\mathbf{h}_0 = \mathbf{M}_-^{-1}\mathbf{T}^{-1}\mathbf{M}_+\mathbf{h}_1, \tag{10}$$

where the vectors $\mathbf{h}_0 = \{\delta_L, \delta_T, r_L, r_T\}$ and $\mathbf{h}_1 = \{t_L, t_T, 0, 0\}$ are composed of the unknowns r_L, r_T and t_L, t_T, and $\mathbf{M}_-$ and $\mathbf{M}_+$ are the matrixes defined by Eq. (9) for the lower and the upper half-plane, respectively.

The coefficients t_L and t_T are determined from the first two equations in the system (10), while the coefficients r_L and r_T are explicitly expressed in terms of t_L and t_T. Collecting the powers

of the eigenvalues in the solution, which are diagonal elements of the matrix $\mathbf{\Lambda}^N$, leads to the series expansion

$$\{t_L, t_T\} = \sum_{i=1}^{4} \mathbf{m}_i \lambda_i^N / \Delta,$$
$$\Delta = \sum_{i=1}^{3} \sum_{j=i+1}^{4} \Delta_{ij} \lambda_i^N \lambda_j^N. \tag{11}$$

Here, the eigenvalues have the relations $\lambda_3 = 1/\lambda_1$ and $\lambda_4 = 1/\lambda_2$, while the vectors $\mathbf{m}_i = \{m_{iL}, m_{iT}\}$ and the coefficients Δ_{ij} $(i,j = 1,2,3,4)$ are expressed in terms of the matrices $\|d_{ij}\| = \mathbf{M}_-^{-1}\mathbf{G}^{-1}$ and $\|e_{ij}\| = \mathbf{G}\mathbf{M}_+$ as

$$\mathbf{m}_i = (d_{2i}\delta_L - d_{1i}\delta_T)\{e_{i2} - e_{i1}\},$$

$$\Delta_{ij} = \begin{vmatrix} d_{1i} & d_{1j} \\ d_{2i} & d_{2j} \end{vmatrix} \cdot \begin{vmatrix} e_{i1} & e_{i2} \\ e_{j1} & e_{j2} \end{vmatrix}.$$

The reflection coefficients of the plane waves

$$\{r_L, r_T\} = \sum_{j=1}^{3} \sum_{k=j+1}^{4} \mathbf{s}_{jk} \lambda_j^N \lambda_k^N / \Delta$$

are expressed in terms of the components of the vector $\mathbf{s}_{jk} = \{s_{1jk}, s_{2jk}\}$, which is given by

$$s_{ijk} = (e_{j1}e_{k2} - e_{j2}e_{k1})\left[(d_{i+2\,j}d_{2k} - d_{i+2k}d_{2j})\delta_L - (d_{i+2\,j}d_{1k} - d_{i+2k}d_{1j})\delta_T\right],$$
$i = 1,2;\ j,k = 1,2,3,4.$

2.5. Mathematical model for functionally graded phononic crystals

The T-matrix method can be exploited for the analysis of FG phononic crystals in a similar manner to the procedure described above. Let us consider the i-th unit-cell of the FG phononic crystal occupying the region $a_{i-1} \leqslant z \leqslant a_i,\ |x| < \infty$ as shown in Figs. 1 and 2. It is composed of the homogeneous layers A and B of the thicknesses h_A and h_B and two FG interlayers (AB, BA) of the thickness h_F. Thus, the T-matrix for the unit-cell is given by

$$\mathbf{T}_c = \mathbf{T}(z_{BA}, z_B)\mathbf{T}(z_B, z_{AB})\mathbf{T}(z_{AB}, z_A)\mathbf{T}(z_A, z_0),$$

where $z_0 = a_{i-1},\ z_A = z_0 + h_A,\ z_{AB} = z_A + h_F,\ z_B = z_{AB} + h_B$ and $z_{BA} = z_B + h_F = a_i$ are the z-coordinates of the boundaries of the corresponding layers. Here, $\mathbf{T}(z_A, z_0)$ and $\mathbf{T}(z_{BA}, z_B)$ are the T-matrices of the homogeneous elastic layers that have explicit expressions derived from Eq. (8). The T-matrices for FG interlayers $\mathbf{T}(z_{AB}, z_A)$ and $\mathbf{T}(z_B, z_{AB})$ have to be evaluated numerically except some particular cases, e.g., exponential laws or special power laws (Han and Liu, 2002) for the material gradation.

A simple layer model (LM) for the FG layer is used further. In the LM, the T-matrix of the FG layer is approximated by the product of the T-matrices for M homogeneous sub-layers (Fig. 1(b)) as

$$\mathbf{T}(z_{AB}, z_A) \approx \prod_{i=M}^{1} \mathbf{T}(z_i, z_{i-1}), \quad \mathbf{T}(z_{BA}, z_B) \approx \prod_{i=M}^{1} \mathbf{T}(z'_i, z'_{i-1}),$$

$$z_0 = z_A, \quad z_L = z_{AB}, \quad z_i = z_0 + h(i-1), \quad i = 1,2,\ldots,M,$$

$$z'_0 = z_B, \quad z'_L = z'_{BA}, \quad z'_i = z'_0 + h(i-1), \quad i = 1,2,\ldots,M,$$

where $h = h_F/(M-1)$.

In the numerical calculations, normalized parameters are introduced for convenience. The length parameter equal to the thickness of the unit-cell H and the shear wave velocity $c_A = \sqrt{\mu_A/\rho_A}$ of material A are used for normalization. Accordingly, the normalized frequency is defined by $\Omega = \omega H/(2\pi c_A)$.

Numerical studies have shown that with increasing number of sub-layers, the relative error in the calculated band-gaps decreases. In particular, our numerical experiments have demonstrated that $M = 200$ sub-layers are more than enough to achieve convergent results. An example of the convergence study of the calculated band-gaps for incident P- and SV-waves is shown in Fig. 3 for $h_A/h_B = 1,\ h_F/H = 0.5$ and $\theta = 40^\circ$. The numerical results are indistinguishable by eye if $M > 60$. Here, the colored and the dashed domains in the sub-plots are band-gaps which will be discussed in the next section in details.

2.6. Classification of band structures

The most interesting phenomenon of phononic crystals is the existence of band-gaps or stop-bands. Band-gaps are frequency ranges, where the transmission of elastic waves or mechanical energy through the periodic structure is impossible. All other frequency ranges, in which a non-zero wave transmission is observed, are called pass-bands. In the present investigation, oblique wave incidence is also considered. Band-gaps valid for all incidence angles are often denoted as full or complete band-gaps. It is important to note here, that periodic structures with a finite number of unit-cells are considered here. Accordingly, the definition of band-gaps here differs slightly from the band-gap definition for infinite phononic crystals.

Band-gaps (BG) correspond to the frequencies of a full wave blocking if $N \to \infty$. The transmission coefficient decreases in the band-gaps exponentially with the number of the unit-cells. Another situation does not fully correspond to band-gaps, but it is also sufficiently different from pass-bands. These are frequency ranges where the wave transmission is very low, but the

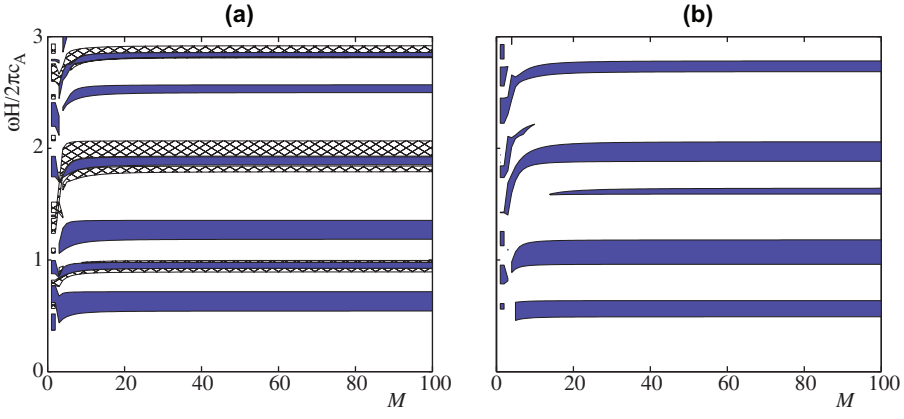

Fig. 3. Band-gap convergence with increasing number M of the homogeneous sub-layers to approximate the FG sub-layers for incident P-wave (a) and S-wave (b) at an angle $\theta = 40^\circ$.

transmission coefficient does not tend to 0 at $N \to \infty$. Such frequency ranges are designated in this analysis as low transmission pass-bands (LTPB), where the wave transmission is very low, but however a full wave blocking does not exist. More details and discussions on LTPB are given in the following.

2.6.1. Wave energy transmission and reflection coefficients

The energy transmission coefficient κ^+ and the energy reflection coefficient κ^- are usually introduced in order to characterize the energy flow transfer in the laminated composites (Glushkov and Glushkova, 1997). The energy transmission coefficient κ^+ is defined as the ratio of the time-averaged energy flow transmitted through the composite to the energy of the incident waves (e.g., Golub et al., 2012b). According to the energy conservation law, the energy balance equation $\kappa^+ + \kappa^- = 1$ should be satisfied, which is used as a check during the simulation in order to validate the correctness and the accuracy of the numerical results.

The energy transmission coefficient κ^+ is a convenient tool to analyze band-gaps and pass-bands of the multi-layered periodic composite structure under consideration. Frequency ranges wherein the energy transmission coefficient $\kappa^+ \to 0$ exponentially at $N \to \infty$ correspond to band-gaps. Frequency ranges, wherein the transmission coefficient has a non-zero value, represent the so-called pass-bands. The numerically calculated energy transmission coefficient can be used to identify whether the frequencies under consideration belong to band-gaps or pass-bands. But the identification between full and partial band-gaps demands extra calculations for different N.

2.6.2. Identification and classification of band-gaps using the eigenvalues of the T-matrix

The eigenvalues of the T-matrix are used to classify the band structure. For simplicity, the eigenvalues λ_1 and λ_2 of the transfer matrix $\mathbf{T}_c$ are ordered in accordance with the inequality $|\lambda_2| \geqslant |\lambda_1| \geqslant 1$. The analysis of the expression (11) for the transmission coefficients at $N \to \infty$ shows evidently that the pass-band corresponds to $|\lambda_2| = |\lambda_1| = 1$. In other cases the asymptotics of the transmission coefficients

$$\{t_L, t_T\} \sim (\mathbf{m}_1 \lambda_2^{-N} + \mathbf{m}_2 \lambda_1^{-N})/(\Delta_{12} + \Delta_{23}\lambda_1^{-2N}), \quad \text{at } N \to \infty$$

reveals three different situations for the band structure when $|\kappa^+| \ll 1$, which are given in Table 2.

The first two rows in Table 2 show a fast exponential decay of κ^+ at $N \to \infty$ and they are denoted as band-gaps or stop-bands. Here, the notation $f = O(u)$ at $x \to a$ is used to denote that $f(x)$ and $u(x)$ are infinitesimal functions of the same order, i.e., $f \sim Au,\ 0 < |A| < \infty$. In order to gain a deeper insight into the band structure, the band-gaps are classified as band-gaps of 1. kind (BG-I) and 2. kind (BG-II). It should be noted that the present definition of band-gaps by using eigenvalues of the T-matrix is in agreement with the concept of localization factors defined by the smallest positive Lyapunov exponent (Castanier and Pierre, 1995). For checking the correctness of the present band-gap definition, a comparison with the results based on the localization factors given in Chen and Wang (2007) has been made. A good agreement has been obtained though different numerical procedures have been used. Unlike the present investigation, no FG interlayers and no low transmission pass-bands (LTPB) were considered in Chen and Wang (2007). From the physical point of view, the localization factor γ is equal to the factor of the exponential decay of the wave field as $e^{-\gamma N}$. Thus the localization factor is $\gamma = \gamma_1$ if $\mathbf{m}_2 \neq \mathbf{0}$ and $\gamma = \gamma_2$ if $\mathbf{m}_2 = \mathbf{0}$ within the band-gabs ($\gamma_{1,2}(\omega) = \log|\lambda_{1,2}|$), see Table 2. In contrast, the wave amplitude has no exponential decay within the pass-bands, so the localization factor is equal to zero, i.e., $\gamma = 0$.

Band-gaps of 1. kind are determined by the condition $|\lambda_2| \geqslant |\lambda_1| > 1$, which depends on the geometrical and material properties of the unit-cells and the wavenumber. An example of BG-I is given in Fig. 4, where the band-gaps BG-I are marked by yellow rectangles. Fig. 4 shows the dependencies of the transmission coefficient $\kappa^+(\omega)$ and the localization factor $\gamma(\omega)$ and $\gamma_{1,2}(\omega)$ for an incident P-wave at an angle $\theta = 20^\circ$ and for an FG phononic crystal with $h_F = 0.18,\ h_A/h_B = 1$ and $N = 200$.

Band-gaps of 2. kind (BG-II) do not appear so frequently as BG-I and are observed only in some special cases depending on the properties of the unit-cells and the half-planes. For BG-II, the condition $\mathbf{m}_2 = 0$ is satisfied when

$$d_{22}\delta_L - d_{12}\delta_T = 0 \quad \text{or} \quad e_{21} = e_{22} = 0.$$

The second equation is satisfied in some special cases only while the first equation is more natural for the considered FG phononic crystals. It leads to the conclusion that BG-II exist if

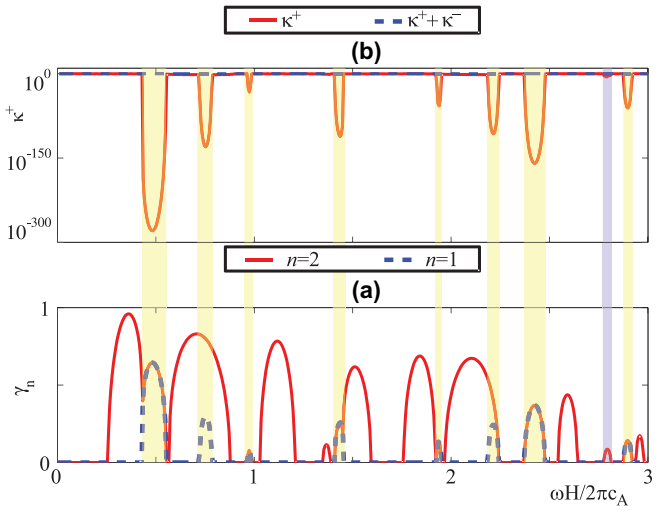

Fig. 4. Dependence of the energy transmission coefficient κ^+ (top) and localization factors $\gamma_n = log(\lambda_n)$ (bottom) corresponding to BG-I (yellow zones) and LTPB (blue zone) for $\theta = 20^\circ,\ h_F = 0.18$ and $h_A/h_B = 1$. (For interpretation of the references to color in this figure legend, the reader is referred to the web version of this article.)

Table 2
Band structure classification.

Type of band	Eigenvalues	Additional conditions	Behavior of κ^+ at $N \to \infty$	Localization factor γ
Band-gap of 1. kind (BG-I)	$\lvert\lambda_2\rvert > 1$ & $\lvert\lambda_1\rvert > 1$	$\mathbf{m}_2 \neq 0$ & $\Delta_{12} \neq 0$ $\mathbf{m}_2 = 0$ & $\Delta_{12} \neq 0$	$\kappa^+ = O(\lvert\lambda_1\rvert^{-2N})$ $\kappa^+ = O(\lvert\lambda_2\rvert^{-2N})$	$\log\lvert\lambda_1\rvert$ $\log\lvert\lambda_2\rvert$
Band-gap of 2. kind (BG-II)	$\lvert\lambda_2\rvert > 1$ & $\lvert\lambda_1\rvert = 1$	$\mathbf{m}_2 = 0$	$\kappa^+ = O(\lvert\lambda_2\rvert^{-2N})$	$\log\lvert\lambda_2\rvert$
Low transmission pass-band (LTPB)	$\lvert\lambda_2\rvert > 1$ & $\lvert\lambda_1\rvert = 1$	$0 < w < \varepsilon < 1$ $w = \lvert\mathbf{m}_2/(\Delta_{12} + \Delta_{23}\lambda_1^{-2N})\rvert$	$\kappa^+ = O(\lvert w\rvert^2)$	0
Pass-band (PB)	$\lvert\lambda_2\rvert > 1$ & $\lvert\lambda_1\rvert = 1$ or $\lvert\lambda_2\rvert = 1$	$w > \varepsilon$	$\kappa^+ = O(1)$	0

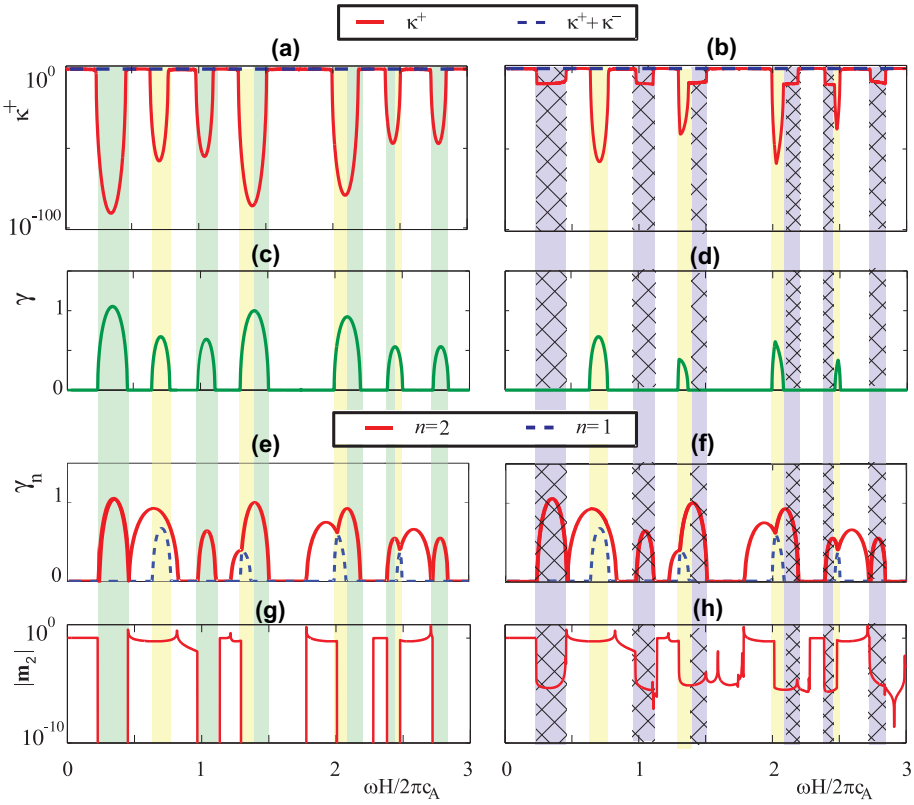

Fig. 5. Transition of BG-II for normally incident SV-wave with $\theta = 0^\circ$ (a,c,e,g) to LTPB for an incidence angle $\theta = 10^{-5}$ (b,d,f,h). Transmission coefficient κ^+ (a,b), localization factor (c,d), eigenvalues (e,f) and amplitudes of the eigenvectors $|\mathbf{m}_k|$ (g,h).

(a) $d_{22} = 0$ and incident P-wave ($\delta_L = 1, \delta_T = 0$),
(b) $d_{12} = 0$ and incident SV-wave ($\delta_L = 0, \delta_T = 1$).

Numerical analysis shows that BG-II can appear only in the case of normally incident waves ($\theta = 0^\circ$). Some examples of BG-II are shown in Fig. 5(a), (c), (e) and (g), where they are marked by cyan rectangles. Here, the geometry of the FG phononic crystal is determined by $h_F = 0.1$ and $h_A/h_B = 1$, and a normally incident SV-wave with $\theta = 0^\circ$ is considered. The coefficient d_{12} is equal to zero within the considered frequency ranges, where $\gamma_2 > 0$ and $\gamma_1 = 0$ which results in BG-II correspondingly.

If $|\lambda_{1,2}| = 1$ then the transmission coefficients are non-zero and oscillate with changing N. The situation is more complicated if $|\lambda_2| > 1$, $|\lambda_1| = 1$ and $|\mathbf{m}_2| \neq 0$. In this case the energy transmission coefficient can be estimated from (11) as $\kappa^+ = O(|w|^2)$ with $w = |\mathbf{m}_2/(\Delta_{12} + \Delta_{23}\lambda_1^{-2N})|$ and the corresponding frequencies

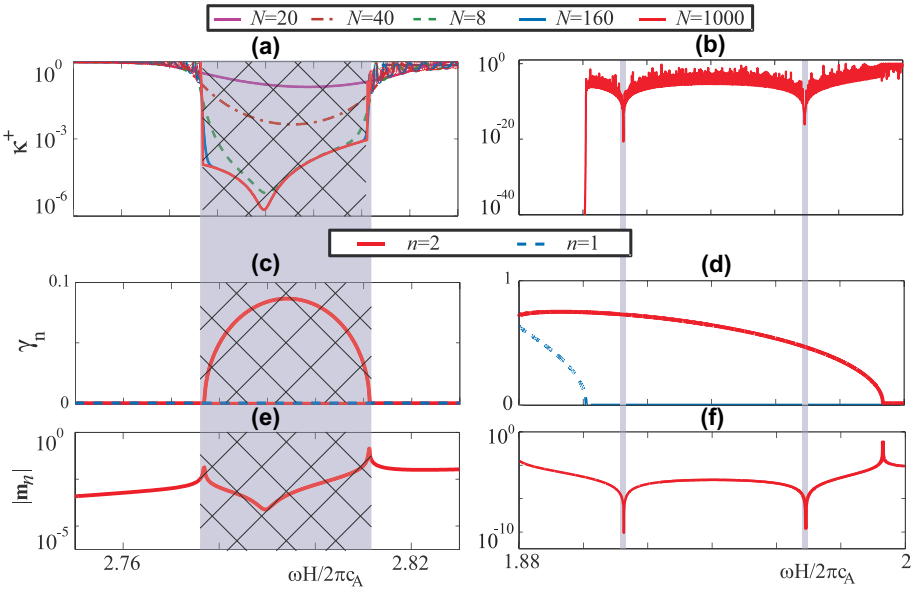

Fig. 6. Transmission coefficient κ^+ (a,b), localization factors $\gamma_n = \log \lambda_n$ (c,d) and amplitudes of the eigenvectors $|\mathbf{m}_n|$ (e,f) for usual LTPB (a,c,e) and point LTPB (b,d,f). Incident P-wave at an angle $\theta = 20^\circ$, $h_F = 0.18$ (a,c,e) and incident SV-wave at an angle $\theta = 40^\circ$ (b,d,f), for $h_F = 0.02$; $h_A/h_B = 1$.

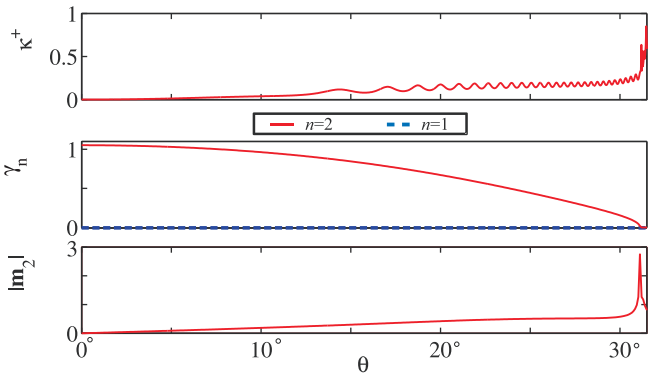

Fig. 7. Transmission coefficient, localization factors and amplitude of the eigenvector $|\mathbf{m}_2|$ in dependence on the angle of incident SV-waves at frequency $\omega H/2\pi c_A = 0.35$ demonstrating the transition of BG-II to LTPB.

belong to pass-bands because of no exponential decay at $N \to \infty$. The asymptotic analysis of (11) does not reveal the behavior of $\kappa^+(N)$, so a complete analysis of $\{t_L, t_T\}$ has been performed. It shows a rather stable decrease at $N \to \infty$ when $|w| < \varepsilon < 1$ as shown in Fig. 6(a), (c) and (e). Here, the value $\varepsilon = 0.3$ has been chosen so that $\kappa^+ < 0.1$ with $N \geqslant 200$. Of course, the width of LTBP depends on the value of ε, but LTPB shrinks slowly with decreasing ε, e.g. Fig. 5(a). According to our careful analysis, pass-bands can be classified into two categories, namely, normal pass-bands and low transmission pass-bands (LTPB), where the wave transmission in the phononic crystal is quite low but not zero.

It should be noted that the LTPB occur at non-zero incidence angles only and they arise usually from BG-II. The consideration of an arbitrary incidence angle like in the present investigation demands some comments and examples about the relation between the solutions for normal incidence and oblique incidence. The transition of the BG-II (cyan ranges of left sub-plots) to the LTPB (blue ranges of right sub-plots) is demonstrated in Fig. 5. Though there is a jump in the localization factor from zero to a certain small non-zero angle due to the special asymptotic behavior, the other quantities of the solution (the energy transmission coefficient κ^+, the eigenvalues λ_k, and $|\mathbf{m}_k|$ etc.) are smooth functions of θ. An example is given in Fig. 7 for the first BG-II, which is depicted in Fig. 5(a) at $\omega H/2\pi c_A = 0.35$. It is clearly seen from Fig. 7 that for small incidence angles $(0 \leqslant \theta < 10^\circ)$ $|\mathbf{m}_2|$ is a linear function of θ at frequencies within BG-II and LTPB. The energy transmission coefficient has an asymptotic form of $\kappa^+ = O(A\exp(-2\gamma_2 N) + \theta^2)$ at $N \to \infty$ and $\theta \to 0^\circ$ where A is a constant. Thus, the localization factor $\gamma = \gamma_2$ at $\theta = 0^\circ$ corresponds to BG-II. Besides, Fig. 7 shows the evolution of LTPB into PB with changing incidence angle. The transmission coefficient is quite small for the considered incidence angles where $\gamma_2 > 0$, and it reaches the value 1 only if $\gamma_2 = 0$.

The occurrence of LTPB with the increasing number of unit-cells is demonstrated in Fig. 6(a). The left column of the sub-plots is a

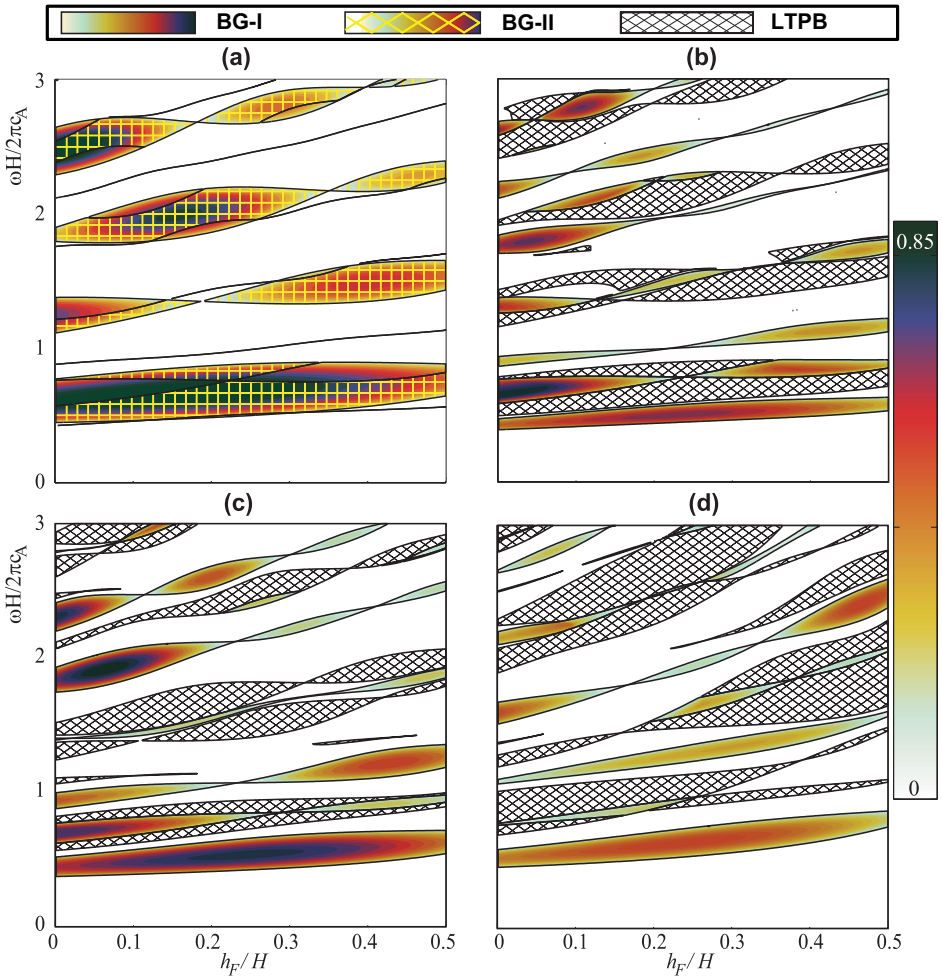

Fig. 8. Influence of the relative thickness of FG interlayers h_F/H on band-gaps for incident P-waves at angles $\theta = 0^\circ$ (a), $\theta = 20^\circ$ (b), $\theta = 40^\circ$ (c) and $\theta = 80^\circ$ (d), and for $h_A/h_B = 1$.

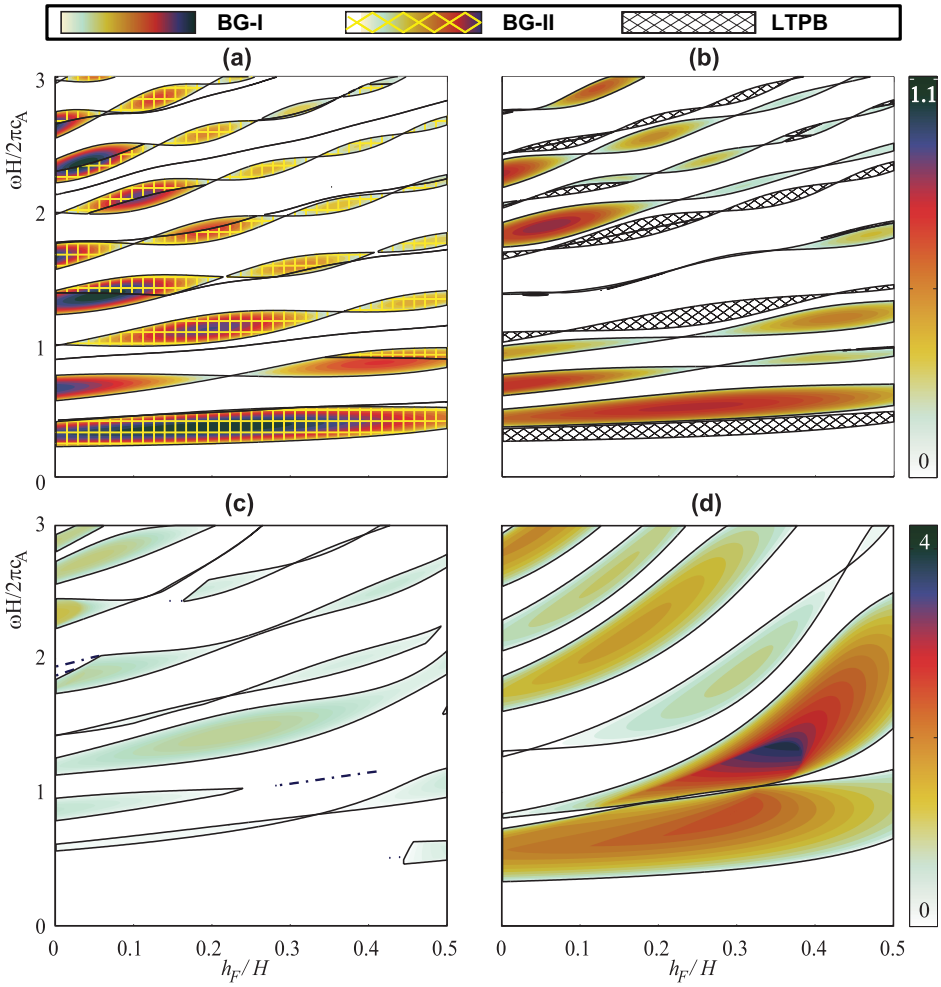

Fig. 9. Influence of the relative thickness of FG interlayers h_F/H on band-gaps for incident SV-waves at angles $\theta = 0^\circ$ (a), $\theta = 20^\circ$ (b), $\theta = 40^\circ$ (c) and $\theta = 80^\circ$ (d), and for $h_A/h_B = 1$.

zoom of Fig. 4. Starting from $N = 160$, the level of the transmission coefficient is quite small, but not less than 10^{-6}. It should be mentioned here that the LTPB are not band-gaps exactly specking, but within such LTPB the wave transmission through the phononic crystal is practically forbidden. A parametrical study shows some special cases where point LTPB occur for certain incidence angles. For instance, at $\theta = 40^\circ$ the LTPB degenerate into a point if $h_f = 0.02$, $h_A/h_B = 1$ and $\theta = 40^\circ$ as shown in Fig. 6(b).

3. Numerical results and discussions

The existence of band-gaps, their width and location are important for engineering applications. They can be utilized for the design of novel acoustic devices such as wave filters, tools for selective generation, muting etc. From the standpoint of operating modes of such devices the appropriate parameters should be chosen for wave excitation as carrier frequency, type and incidence angle of incident waves as well as material properties. Both geometrical and material parameters of phononic crystals strongly influence the width and the location of band-gaps.

In this section the influences of the thicknesses of the homogenous layers and FG interlayers in the unit-cell as well as the incident wave on band-gaps are analyzed. Band-gap diagrams are used to show the variation of band-gaps with the variation of geometrical and material parameters. Different types of band-gaps and pass-bands are marked in different ways in Figs. 8–12. Graded domains are band-gaps of 1. kind (BG-I), the gradually colored domains with light hatching are band-gaps of 2. kind (BG-II), low transmission pass-bands (LTPB) with a transmission coefficient $\kappa^+ < 0.1$ are denoted by hatching only, and purely white domains correspond to pass-bands.

The color intensity for BG-I and BG-II is given in accordance with the localization factor γ within the stop-band. The value of the localization factor is shown by a corresponding color, and the last column in each figure shows the localization factor in the band-gaps. In some cases the width of the LTPB is very small and therefore such "point" band-gaps are denoted by dashed lines.

3.1. Influence of the FG interlayers on band-gaps

Functionally graded interlayers may have significant influences on the elastic wave propagation in layered periodic phononic crystals. The dependence of the band structure on the relative thickness of FG interlayers h_F/H for incident P-waves at incidence angles $\theta = 0^\circ$, $\theta = 20^\circ$, $\theta = 40^\circ$ and $\theta = 80^\circ$ is shown in Fig. 8 for $h_A/h_B = 1$. The band-gap diagrams for incident SV-waves at the same incidence angles as in Fig. 8 are given in Fig. 9. Obviously, $h_F = 0$ corresponds to the case of a phononic crystal composed of homogenous elastic layers only. The band-gaps shift to higher frequencies with increasing h_F/H. Usually the width of the first band-gap at low frequencies (see for example Fig. 8(a)) depends weakly on h_F, while the width of high-frequency band-gaps changes more strongly with h_F/H and it may shrink to zero in certain cases.

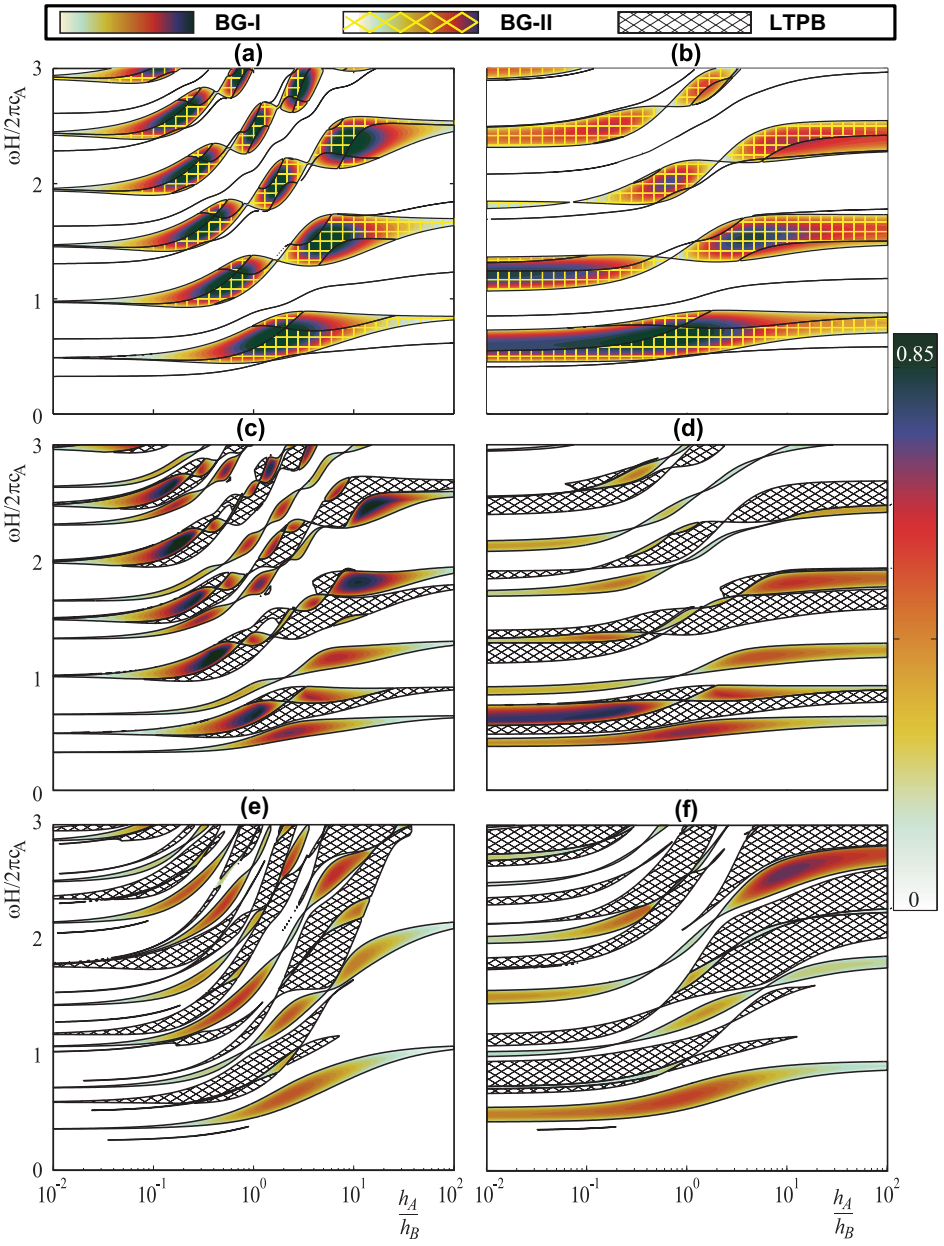

Fig. 10. Influence of the thickness ratio of homogenous layers h_A/h_B (in logarithmic scale) on band-gaps in phononic crystals without FG interlayers ($h_F = 0$, first column) and with FG interlayers ($h_F = 0.25$, second column) for incident P-waves at various incidence angles $\theta = 0^\circ$ (first row), $\theta = 20^\circ$ (second row) and $\theta = 80^\circ$ (third row).

Some point band-gaps are observed in these figures. The term "point stop-band" is used here for the case of an infinitesimally small width in the frequency domain for fixed parameters of the phononic crystal. No transmission of the wave energy is possible at the frequency belonging to the point BG-I, and it is observed for normal wave incidence ($\theta = 0^\circ$), see continuous lines and points of shrinking zone in Figs. 8(a) and 9(a). Point LTPB, in which the transmission coefficient is $\kappa^+ < 10^{-5}$, are shown in Fig. 9(c) by dashed lines.

If the incidence angle deviates from zero, then BG-II change over to LTPB as shown in Fig. 5. Therefore we can observe the two different types of band-gaps in Fig. 8(b)–(d). Some BG-I exist in consolidation with LTPB. These consolidation continuously changes with the variation of the relative thickness of FG interlayers and the incidence angle. Furthermore, some BG-I appear only in FG phononic crystals, e.g., see BG-I in the range of $2 < \omega < 2.2$ and $0.05 < h_F < 0.2$ in Fig. 8(b). However, these BG-I exist in a consolidation with the LTPB. Other BG-I appear in the diagrams without contiguity to the LTPB, e.g., see BG-I in Fig. 8(b). Interestingly, the eigenvalue λ_1 is the complex conjugate to λ_2 within these zones, and the corresponding LTPB evolve from the point BG arising at $\theta = 0^\circ$ as shown Fig. 8(a).

The corresponding band-gaps for incident SV-waves are presented in Fig. 9. In contrast to incident P-waves, here the LTPB disappear with increasing incidence angle. For example, the LTPB become the point LTPB at an incidence angle $\theta = 40^\circ$ as shown in Fig. 9(c) by dashed lines. With further increasing incidence angle, the BG become wider, and the localization factor increases (see Fig. 9(d)).

3.2. Influence of the homogeneous layers on band-gaps

In order to investigate the influence of the geometrical parameters of the phononic crystal, the thickness ratio $K = h_A/h_B$ of the

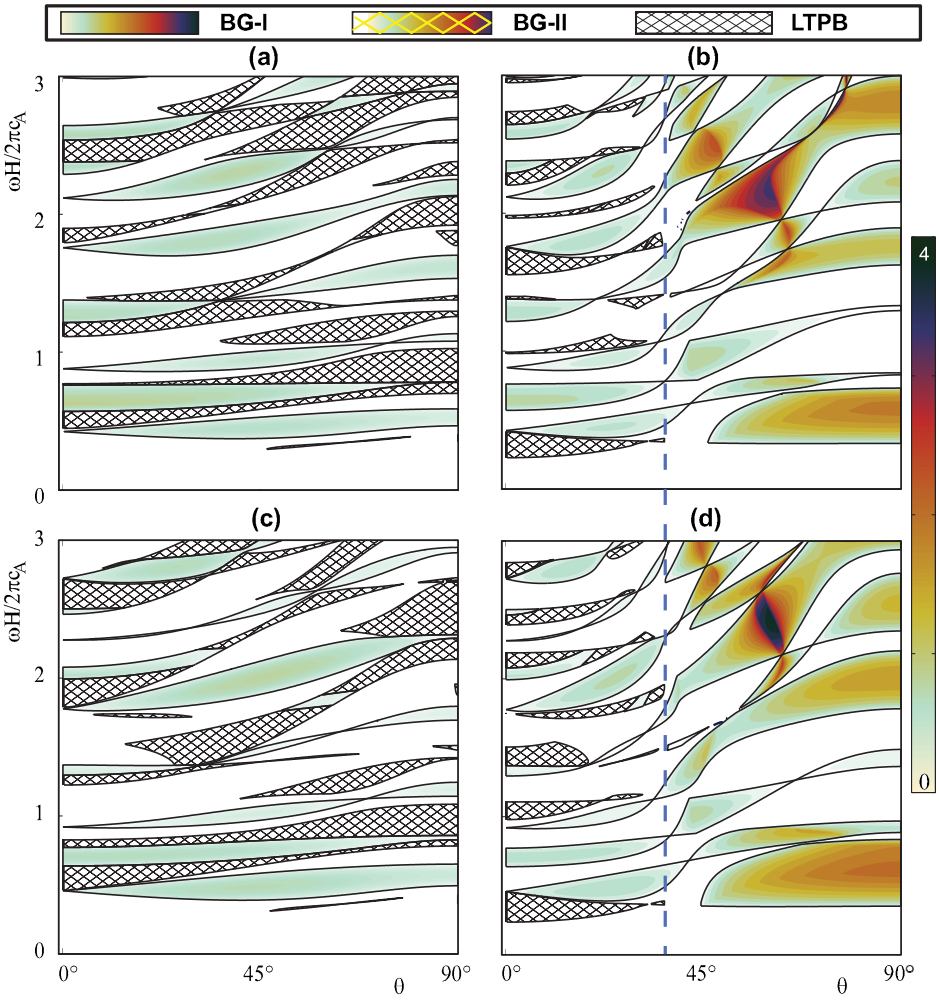

Fig. 11. Band-gap diagrams in dependence on the incidence angle of incident P- (first column) or SV-waves (second column) for $h_A/h_B = 1$ and two thicknesses of FG interlayers $h_F = 0$ (first row), $h_F = 0.1H$ (second row).

homogenous layers A and B of the unit-cells of the considered periodic structure is introduced. Fig. 10 depicts band-gap dependence on the ratio K in logarithmic scale. Here, incident P-waves at four different incidence angles $\theta = 0^\circ, 20^\circ, 40^\circ, 80^\circ$ are considered for phononic crystals without FG interlayers ($h_F = 0$) and with FG interlayers of a thickness $h_F = 0.25H$. When the angle of the incident P-wave increases the maximum of the localization factor in the band-gaps decreases, but the LTPB widen on the contrary.

Fig. 10 shows that the band-gaps change within the range $10^{-1} < K < 10$, where their form, width and position depend strongly on K. The band-gaps draw up to the gradually tapering zones and their localization factors tend to zero when $K \to 0$ or $K \to \infty$ since the corresponding phononic crystal becomes a homogeneous structure. Opposite to phononic crystals composed of homogeneous layers only, the band-gaps in the FG phononic crystals do not disappear at $K \to 0$ or $K \to \infty$ since the structure in these cases remains periodically heterogeneous. With increasing thickness or volume fraction of the hard material A, the band-gaps move to higher frequencies. When the fraction of the hard material A is larger than that of the soft material B ($K > 10$), the band-gaps are wider than in opposite case $K < 10^{-1}$, see Fig. 10. The presence of the soft material B, even at a low volume fraction with $h_A = 100h_B$, may significantly affect the band-gaps in the layered phononic crystal without FG interlayers. This conclusion is well known from early literature on elastic wave propagation (Achenbach, 1973; Auld, 1973).

3.3. Influence of the wave incidence on band-gaps

Next, the influences of the type and incidence angle of incident elastic waves on the wave propagation in phononic crystals are analyzed. The changes of the band-gap diagrams from layered ($h_F = 0$) to functionally graded ($h_F/H = 0.1, 0.25$ and 0.5) phononic crystals can be observed in Figs. 11 and 12. Even quite thin FG interlayers with $h_F = 0.1H$ result in different band-gaps and LTPB compared with that for layered phononic crystals without FG interlayers, especially in the high-frequency range. Generally, the band-gaps do not disappear as the incidence angle varies. The BG-I can disappear at some incidence angles and change over to LTPB, so that the bands with a small transmission coefficient $0 \leqslant \kappa^+ < 0.1$ are overall continuous. All LTPB starting from a small incidence angle $\theta \neq 0^\circ$ evolve from the corresponding BG-II for the normal incidence with $\theta = 0^\circ$.

By analyzing the BG-I carefully it can be noted that the band-gaps in the diagrams of the first columns (incident P-wave) are similar to that in the second columns (incident SV-wave) at $|\theta| < \theta^*$, $\theta^* \approx 36^\circ$, if the first are properly scaled, see domains before the dashed vertical lines in Figs. 11, 12(b) and (d). It becomes obvious if we notice that all BG-I are invariant with respect to the

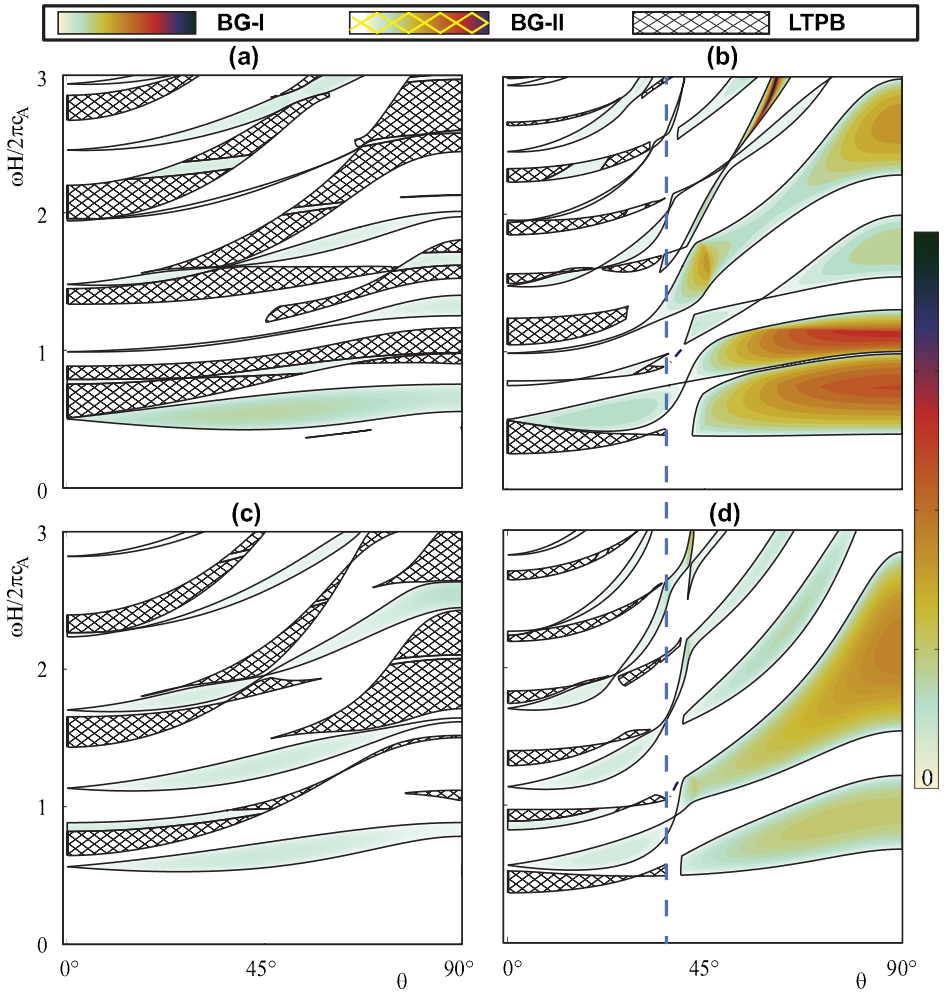

Fig. 12. Band-gap diagrams in dependence on the incidence angle of incident P- (first column) and SV-waves (second column) for FG phononic crystals with $h_F = 0.25H$ (fist row) and $h_F = 0.5H$ (second row).

quantity $\varkappa \sin\theta$ of the incident wave. So for any incidence angle θ_P of the incident P-waves, there is a specific angle θ_S of the incident SV-waves when their BG-I are identical. The relationship between both incidence angles is governed by the following Snell's law

$$\varkappa_S \sin\theta_S = \varkappa_P \sin\theta_P.$$

On the contrary, any BG-I for incident SV-waves with an incidence angle of $|\theta_s| > \theta^*$ where $\theta^* = \arcsin(\varkappa_P/\varkappa_S)$ is also forbidden incident P-waves. Besides, band-gaps for $|\theta| > \theta^*$ are more "robust" (in the sense that the corresponding localization factors are larger) and wider than that for small incidence angles, LTPB are not observed, see second columns of Figs. 11 and 12.

4. Conclusions

In this paper, propagation and band-gaps of time-harmonic plane elastic P- and SV-waves in periodically laminated composites or 1D phononic crystals composed of homogeneous layers and FG interlayers are analyzed. The FG interlayers are approximated by using a simple multi-layer model, and the convergence of the method is demonstrated. The present investigation is mainly focused on efficient and accurate methods for the calculation of band-gaps in 1D FG phononic crystals, but the methods can be easily extended to 1D piezoelectric phononic crystals, which have wide-range innovative applications (Gomopoulos et al., 2010; Chen et al., 2013).

A modified classification of band-gaps in 1D phononic crystals is proposed. The classification relies on the exact analysis of the eigenvalues of the transfer matrix for a unit-cell and the asymptotics of the transmission coefficient. In particular, two kinds of band-gaps are specified as BG-I and BG-II. Within the band-gaps the transmission coefficient decays exponentially with the number of the unit-cells tending to infinity. The term "low transmission pass band" (LTPB) is introduced in order to identify frequency ranges, where the transmission coefficient is not exactly zero but sufficiently small and negligible for practical engineering applications of phononic crystals. BG-I diagrams bend and change continuously with varying geometrical and material parameters as well as the wave incidence angle, but for BG-II the same tendency is valid only for normally incident waves ($\theta = 0°$). When θ increases from zero, BG-II turn into LTPB.

Numerical results show that the width and the location of the band-gaps are strongly dependent on the relative thickness of the homogeneous layers, the thickness of the FG interlayers, the material properties, and the type and incidence angle of incident elastic waves. It is revealed that band-gaps shift to higher frequencies and pass-bands widen with the increasing thickness of FG interlayers. The transition of BG-II to LTPB for different parameters of phononic crystals are investigated in details. BG-II exist only in the case of normally incident elastic waves, and they change over into LTPB when the incidence angle is larger than zero.

Acknowledgments

The authors are grateful to Professors E.V. Glushkov and N.V. Glushkova for fruitful discussions. The work is supported by the Ministry of Education and Science of Russian Federation (11.9157.2014), Russian Foundation for Basic Research (Project 14-01-31236) and the German Academic Exchange Services (DAAD) which are gratefully acknowledged.

References

Achenbach, J.D., 1973. Wave Propagation in Elastic Solids. North-Holland Publishing Company, Amsterdam–London.
Aizikovich, S., Krenev, L., Sevostianov, I., Trubchik, I., Evich, L., 2011. Evaluation of the elastic properties of a functionally-graded coating from the indentation measurements. ZAMM J. Appl. Math. Mech./Z. Angew. Math. Mech. 91, 493–515.
Aki, K., Richards, P.G., 2002. Quantitative Seismology, second ed. University Science Books.
Alleyne, D.N., Cawley, P., 1992. The interaction of lamb waves with defects. IEEE Trans. Ultrason. Ferroelectr. Freq. Control 1, 381–397.
Auld, B.A., 1973. Acoustic Fields and Waves in Solids, vol. 2. Wiley, New York.
Babeshko, V., Glushkov, E., Glushkova, N., 1987. Methods of constructing green's matrix of a stratified elastic half-space. USSR Comput. Math. Math. Phys. 27, 60–65.
Berezovski, A., Engelbrech, J., Maugin, G.A., 2003. Numerical solution of two dimensional wave propagation in functionally graded materials. Eur. J. Mech. A/Solids 22, 257–265.
Brekhovskikh, L.M., Godin, O.A., 1998. Acoustics of layered media. I. Plane and quasi-plane waves. Springer, Berlin/Heidelberg.
Brillouin, L., 1946. Wave Propagation in Periodic Structures. McGraw-Hill, New York.
Castanier, M., Pierre, C., 1995. Lyapunov exponents and localization phenomena in multi-coupled nearly periodic systems. J. Sound Vib. 183, 493–515.
Chakraborty, A., Gopalakrishnan, S., 2003. A spectrally formulated finite element for wave propagation analysis in functionally graded beams. Int. J. Solids Struct. 40, 2421–2448.
Chen, A.L., Wang, Y.S., 2007. Study on band gaps of elastic waves propagating in one-dimensional disordered phononic crystals. Phys. B: Condens. Matter 392, 369–378.
Chen, Z., Yang, Y., Lu, Z., Luo, Y., 2013. Broadband characteristics of vibration energy harvesting using one-dimensional phononic piezoelectric cantilever beams. Phys. B: Condens. Matter 410, 5–12.
Gilbert, F., 1983. Propagator matrices in elastic wave and vibration problems. J. Acoust. Soc. Am. 73, 137–142.
Glushkov, E.V., Glushkova, N.V., 1997. Blocking property of energy vortices in elastic waveguides. J. Acoust. Soc. Am. 102, 1356–1360.
Glushkov, E.V., Glushkova, N.V., Fomenko, S.I., Zhang, C., 2012. Surface waves in materials with functionally gradient coatings. Acoust. Phys. 58, 339–353.
Golub, M.V., Fomenko, S.I., Bui, T.Q., Zhang, C., Wang, Y.S., 2012a. Transmission and band gaps of elastic SH waves in functionally graded periodic laminates. Int. J. Solids Struct. 49, 344–354.
Golub, M.V., Zhang, C., Wang, Y.S., 2012b. SH-wave propagation and scattering in periodically layered composites with a damaged layer. J. Sound Vib. 331, 1829–1843.
Golub, M.V., Boström, A., Folkow, P.D., 2013. Wave propagation of functionally graded layers treated by recursion relations and effective boundary conditions. Int. J. Solids Struct. 50, 766–772.
Gomopoulos, N., Maschke, D., Koh, C.Y., Thomas, E.L., Tremel, W., Butt, H.J., Fytas, G., 2010. One-dimensional hypersonic phononic crystals. Nano Lett. 10, 980–984.
Grinchenko, V.T., Meleshko, V.V., 1981. Harmonic Vibrations and Waves in Elastic Bodies. Naukova Dumka, Kiev.
Han, X., Liu, G.R., 2002. Effects of SH waves in a functionally graded plate. Mech. Res. Commun. 29 (5), 327–338.
Han, X., Liu, G.R., Lam, K., 2001. Transient waves in plates of functionally graded materials. Int. J. Numer. Methods Eng. 52, 851–865.
Haskell, N., 1953. The dispersion of surface waves in multi-layered media. Bull. Seismol. Soc. Am. 43, 17–34.
Jha, D., Kant, T., Singh, R., 2013. A critical review of recent research on functionally graded plates. Compos. Struct. 96, 833–849.
Ke, L., Wang, Y., 2006. Two-dimensional contact mechanics of functionally graded materials with arbitrary spatial variations of material properties. Int. J. Solids Struct. 43, 5779–5798.
Kutsenko, A., Shuvalov, A., Poncelet, O., Norris, A., 2013. Spectral properties of a 2D scalar wave equation with 1D periodic coefficients: application to shear horizontal elastic waves. Math. Mech. Solids 18, 677–700.
Liu, G., Tani, J., Ohyoshi, T., 1991. Lamb waves in a functionally gradient material plates and its transient response. Part I: Theory. Trans. Japan Soc. Mech. Eng. 57, 603–608.
Liu, G., Han, X., Lam, K., 1999. Stress waves in functionally gradient materials and its use for material characterization. Compos. Part B: Eng. 30, 383–394.
Maldovan, M., Thomas, E.L., 2009. Periodic Materials and Interference Lithography for Photonics, Phononics and Mechanics. Wiley-VCH Verlag GmbH & Co. KGaA, Weinheim, Germany.
Matsuda, O., Glorieux, C., 2007. A green's function method for surface acoustic waves in functionally graded materials. J. Acoust. Soc. Am. 121, 3437–3445.
Petrashen, G., 1952. Propagation of elastic waves in stratified isotropic media separated by parallel planes. Uch. Zap. LGU 162, 3–189 (in Russian).
Saini, G., Pezeril, T., Torchinsky, D.H., Yoon, J., Thomas, E., Nelson, K., 2007. Pulsed laser characterization of multicomponent polymer acoustic and mechanical properties in the sub-ghz regime. J. Mater. Res. 22, 719–723.
Santare, M., Thamburaj, P., Gazonas, G., 2003. The use of graded finite elements in the study of elastic wave propagation in continuously nonhomogeneous materials. Int. J. Solids Struct. 40, 5621–5634.
Sato, Y., 1959. Numerical integration of the equation of motion for surface waves in a medium with arbitrary variation of material constants. Bull. Seismol. Soc. Am. 49, 57–77.
Shen, H.S., 2009. Functionally Graded Materials: Nonlinear Analysis of Plates and Shells. CRC Press Taylor & Francis Group, USA.
Shuvalov, A., Poncelet, O., Deschamps, M., Baron, C., 2005. Long-wavelength dispersion of acoustic waves in transversely inhomogeneous anisotropic plates. Wave Motion 18, 367–382.
Sobczak, J., Drenchev, L., 2013. Metallic functionally graded materials: a specific class of advanced composites. J. Mater. Sci. Technol. 29, 297–316.
Su, X., Gao, Y., Zhou, Y., 2012. The influence of material properties on the elastic band structures of one-dimensional functionally graded phononic crystals. J. Appl. Phys. 112, 123503.
Thomson, W., 1950. Transmission of elastic waves in stratified solid medium. J. Appl. Phys. 21, 89–94.
Ting, T., 2011. Surface waves in an exponentially graded, general anisotropic elastic material under the influence of gravity. Wave Motion 48, 335–344.
Viktorov, I.A., 1967. Rayleigh and Lamb Waves: Physical Theory and Applications. Plenum Press, New York.
Vollmann, J., Profunser, D., Bryner, J., Dualv, J., 2006. Elastodynamic wave propagation in graded materials: simulations, experiments, phenomena, and applications. Ultrasonics 44, e1215–e1221 (Proceedings of Ultrasonics International (UI05) and World Congress on Ultrasonics (WCU)).
Woo, J., Meguid, S., 2001. Nonlinear analysis of functionally graded plates and shallow shells. Int. J. Solids Struct. 38, 7409–7421.
Wu, M.L., Wu, L.Y., Chen, L.W., 2009. Elastic wave band gaps of one-dimensional phononic crystals with functionally graded materials. Smart Mater. Struct. 18, 115013.
Zubtsov, M., Lucklum, R., Ke, M., Oseev, A., Grundmann, R., Henning, B., Hempel, U., 2012. 2D phononic crystal sensor with normal incidence of sound. Sens. Actuat. A: Phys.186, 118–124.